Electronic structure of molecular-beam-epitaxy growth-induced defects in GaAs

A. C. Beye, B. Gil,* G. Neu, and C. Vèrié
Laboratoire de Physique du Solide et Energie Solaire, Centre National de la Recherche Scientifique, Parc de Sophia Antipolis, rue Bernard Gregory, F-06560 Valbonne, France
(Received 28 April 1987)

The electronic properties of molecular-beam-epitaxy growth-induced defects in GaAs are investigated through a detailed analysis of the 1.504–1.511-eV defect-bound excitons with use of low-temperature photoluminescence, polarization studies, and excitation spectroscopy. It is shown that transfer processes are selective between several high-energy excited states and the low-lying ones, allowing to distinguish at least four sets of bound-exciton complexes related to distinct defect centers. The splitting patterns of the various bound-exciton systems are quantitatively analyzed in the framework of excitons bound to neutral associates, taking into account both J-J coupling and local-field effects. An isoelectroniclike defect model is found to be most consistent with the large splittings in the bound-exciton complexes, the short-range hole-attractive potential of the involved defects, and the angular momentum $J=0$ in the final states of the related transitions.

I. INTRODUCTION

Since the discovery of the excitonic band lying in the 1.504–1.511-eV spectral region (labeled g-v band) on the low-temperature photoluminescence (PL) spectra of GaAs grown by molecular-beam epitaxy (MBE),[1] the remaining problems are the knowledge of their electronic structure and the identification of the involved defects. At first, these emissions were ascribed to the recombination of excitons bound to complex defects whose formation is promoted both by low growth temperature and also interface stoichiometry inherent in the MBE method. Defect models that are based on a closely spaced pairing effect may account for the large number of observed transitions, the selection on the lattice-site separation giving rise to the discrete growth-induced emission lines. The competitive distant donor-acceptor pair (DAP) and bound-exciton (BE) recombination channels[2,3] are typical examples of the various mechanisms that may be responsible for well-resolved fine structures in the optical spectra of semiconductor materials. The BE recombinations imply excitons which are bound to either isoelectronic,[4,5] or donor-acceptor,[6,7] or acceptor-acceptor pairs.[8] Complex defects analogous with nitrogen pairs,[4,5] Cd-O, Zn-O,[6,7] Li-Li-O,[9] and N-B-N pairs[10] in GaP or with isoelectronic Be pairs[11] and Li-Li-C molecular traps[12] in silicon, may be considered in GaAs, for the MBE growth-induced defect. Moreover, in GaAs, Cu-related isoelectronic[13] BE complexes (BEC's) have been evidenced. In addition, high-pressure PL experiments[14] have demonstrated a possible nitrogen contamination of MBE-grown GaAs, thus strengthening an eventual role of N in complex defect associations. The common features of all BEC are (i) a strongly localized exciton, reflecting the importance of central-cell effects and local configuration of the involved centers, and (ii) well-defined and sharp thermodynamic conditions (temperature, stoichiometry, etc.) leading to the defect formation. The complex nature of the growth-induced defects is, in addition, attested to by the polarization properties of several BEC-associated lines.[15–18] The BEC emissions are characteristic of GaAs samples grown by an epitaxial method having various combined *in situ* analysis techniques. Therefore, the study of their electronic structure and also the link between the genesis of the related and well-defined growth conditions is fundamental. It can provide additional information on kinetic processes occurring in the MBE growth in respect to interface stoichiometry. An identification of the involved chemical species has not been achieved until now, although a considerable number of investigations have been reported.[15–34] The main obstacle arises from the inadequacy of the commonly used doping procedures, because the fine structure of the g-v emission band seems well resolved only in the high-purity and p-type sample PL spectra. However, taking into account the anisotropy[35] of the static and dynamic (2×4) As-stable reconstructed GaAs(001) surface, we may expect to have also an anisotropic effect on the completion of oriented defects during the epitaxial growth. As a matter of fact, reflection high-energy electron diffraction[36] (RHEED) and angle-resolved photoemission spectroscopy[37] lead to the conclusion that this surface is more ordered in the $[\bar{1}10]$ direction than in the [110] one. Detailed analysis of the intensity oscillations of RHEED patterns[38,39] has evidenced the presence of surface steps along the $[\bar{1}10]$ direction in a two-dimensional layer-by-layer growth mode.

This paper presents new experimental results of resonant optical spectroscopy and theoretical calculations on the electronic structure of bound-exciton complexes in MBE-grown GaAs. In the following section we describe experimental details. In Sec. III we establish a clear-cut distinction between two kinds of p-type samples, owing to a detailed comparison of their PL spectra: evidence of predominant lines in one kind of PL spectra and suppression of these lines in others. The resonantly excited PL measurements are then presented, with special attention to the selectivity of the *optical excitation transfers* occur-

ring from well-defined upper lines toward low-lying ones. Resonant excitation experiments demonstrate that discrimination between at least four sets of BEC's has to be made to account for the low-energy side of the 1.504–1.511-eV emission band. In the framework of an isoelectronic-like model, involving bound-exciton complexes in local strain fields of low symmetry, explicit calculations are described in Sec. IV, leading to a quantitative fit of the sublevel splittings in each system. Section V is devoted to the description of the different bound-exciton models, focusing the discussion on the isoelectronic BE one. It is shown that this latter model is the simplest one that is consistent in details with the experimental evidence of higher excited states that are related to low-lying ones and an angular momentum $J=0$ in all the final states of the relevant transitions.[18]

II. EXPERIMENT

PL studies are performed at 2K, using a front-surface-layer excitation by a tunable dye laser with Styryl-9 dye, pumped with an argon ionic laser. PL is analyzed by a 1-m-focal-length double monochromator and detected by a photomultiplier tube with a cooled GaAs photocathode. The signal is recorded from a photon-counting system. Luminescence polarization measurements are performed setting a linear polarizer and a quarter-wave retarder with an interlocking gear just before the entrance slit of the monochromator. This experimental arrangement ensures that the results will be unaffected by any anisotropy of the spectrometer and photomultiplier responses. In the same way, the photoluminescence excitation spectra (ES) are recorded as a function of the incident-light polarization using a quarter-wave blade at 45° of the laser-beam polarization and then followed by a linear polarizer allowing the selection of the excitation polarization in any direction of the (001) plane.

About 20 layers grown in a MBE system under standard conditions [i.e., nonintentional doping, growth on (001) As-stabilized surfaces in the 550–600 °C temperature range] and prepared in several laboratories [Thomson, Riber, and Laboratoire de Physique du Solide et Energie Solaire (France), and Max-Planck-Institute (West Germany)] were studied. A comparison of the recorded PL spectra allows one to establish a clear and reproducible classification of the samples into two groups. Excitation experiments were performed on two layers representative of the general properties of each group. They were grown on Cr-doped GaAs substrates using As_4 flux under As-rich conditions ($2<[As_4]/[Ga]<5$). For sample 1, the growth temperature was set at 585 °C using a thermocouple, whereas for sample 2 it was continuously adjusted to 585 °C by an infrared pyrometer measurement in order to compensate for the temperature decrease due to the emissivity variation of the growing sample. The difference between the real substrate temperature and that indicated by the thermocouple has been found to be around 40 °C. Therefore, the growth temperature is assumed to be 550 °C for sample 1. However, in both cases the $[As_4]/[Ga]$ flux ratios and the growth temperatures have yielded As-stabilized (2×4) surface reconstruction. Typical room-temperature mobilities measured for samples 1 and 2 with net acceptor concentrations, respectively, of $p=2\times10^{14}$ and 6×10^{14} cm^{-3} were 400 and 410 cm^2/V s.

III. LOW-LYING STATE SPECTROSCOPY

The PL spectra, reported in Fig. 1 in an expanded scale of the 1.5040–1.5065-eV region, are representative of all the previously published PL spectra of p-type GaAs MBE-grown layers. They may be essentially classified into two groups. The top spectrum (sample 1) is comparable to those obtained by Contour *et al.*[26] and by Skromme *et al.*[33] [Contour-Skromme (CS) type], whereas the bottom spectrum (sample 2) is very close to those recorded by Skolnick *et al.*[17] and by Reynolds *et al.*[28] [Skolnick-Reynolds (SR) type]. The morphology of the g-v emission band is thus closely dependent on the growth conditions. In all n-type samples studied, when the g-v band is detected, this is always a SR-type one. However, at the present time no definite correlation can be made between the growth parameters and the structure of this band. Table I summarizes the energy positions and the corresponding labels previously used in the CS- and SR-type spectra for lines with which we are concerned in the present study. The line relative intensities and polarization behaviors are also reported (as a function of the detection conditions on PL or ES), and will be discussed further in connection with the symmetry of the related centers.

The v_3 and t^* lines at 1.5043_0 and 1.5057_9 eV, respectively, are only detected in the case of the CS-type samples. The other lines are identified in the PL spectra of both samples, even when several emission lines are very

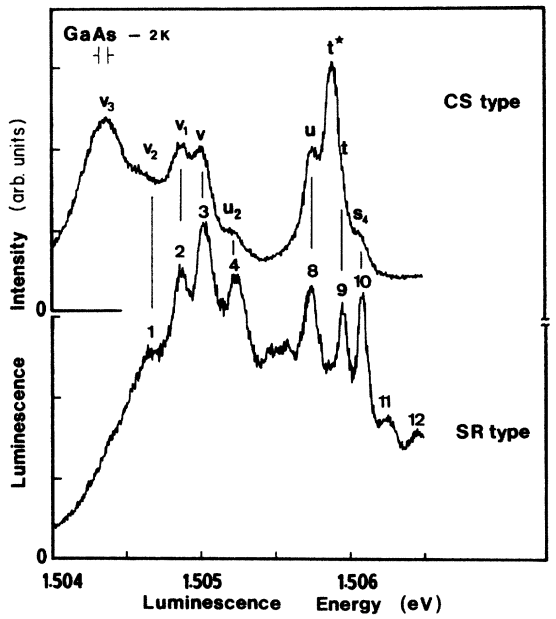

FIG. 1. Photoluminescence spectra on low-energy side of the MBE-growth-induced emission band of GaAs. CS and SR-type spectra were reported, respectively, by Contour *et al.* and Skolnick *et al.* Some lines are identified in both samples, except v_3 and t^*, which are only detected in the CS-type sample. The t^* line was previously labeled t in Refs. 16–26.

TABLE I. List of a part of MBE-growth-induced bound excitons in GaAs reported by Contour *et al.* (Ref. 26) and Skromme *et al.* (Ref. 33) (CS) and by Skolnick *et al.* (Ref. 15) and Reynolds *et al.* (Ref. 28) (SR). Luminescence- (PL) and excitation- (ES) line polarization behaviors are given together with the local symmetry deduced from Zeeman studies (Ref. 18) and from the present quantitative fit of the splitting patterns. The low-lying states down which transfers occur are indicated in the last column. NP denotes not polarized; W denotes weak polarization.

Sample type		Luminescence energy (eV)	Polarization behavior		Local symmetry from		Radiative systems
CS	SR		PL	ES	Ref. 18	This work	
v_3	absent	1.5043_0	[110] W			T_d	
v_2	1	1.5045_8	[110]			C_S	
v_1	2	1.5047_8	[110]			C_{3v}	
v	3	1.5049_3	[110]			C_{2v}	
u_2	4	1.5051_3	[110]				
u	8	1.5056_5	[$\bar{1}$10] W			C_{3v}, C_{2v}	v_1, v
t^*	absent	1.5057_9				T_d	v_3
t	9	1.5058_6	NP	NP		C_s	v_2
s_4	10	1.5059_9	NP	NP			
s	14	1.5066_7	[$\bar{1}$10]	[$\bar{1}$10]	rhombic	C_S	v_2
r	16	1.5069_3	[$\bar{1}$10] W[a]	NP[b]	monoclinic	C_{3v}	v_1
q	17	1.5071_9	[$\bar{1}$10] W		monoclinic	C_{2v}	v
p	19	1.5075_8	[$\bar{1}$10][a]	[$\bar{1}$10][a]	rhombic *I*	C_S	v_2
n	22	1.5080_0	[$\bar{1}$10] W[a]	NP[b]			
k^*	26*a*	1.5087_7		[110][b]		C_S	v_2
k	27	1.5088_1	[$\bar{1}$10]	[$\bar{1}$10]	monoclinic	C_{2v}	v
i^*	29	1.5092_8				C_{2v}	v
i	30	1.5093_4				C_{3v}	v_1
	35	1.5098_0				C_{2v}	v

[a]SR spectrum.
[b]CS spectrum.

weak or appear as shoulders in the CS-type spectrum. For instance, the well-resolved line 9 in the SR-type sample is not defined on the emission spectrum of CS-type layers, but is detected as the t line on excitation spectra.[40] In the same way, lines above 1.5084_5 eV correspond to strong absorbing levels in the CS-type sample, although they are not distinguished on the PL spectrum. The weakness of the high-energy emission lines may result from a thermalization toward the low-energy growth-induced bound excitons. These lines are observed in both type layers at fixed energy and, therefore, for clarity, the letter symbols of Refs. 1 and 16, will be used, followed by the numerical one of Ref. 15 in the following sections. A direct link between several high-energy lines and some low-lying ones is well demonstrated on the PL spectra, selectively excited (SPL) in the energy range of the $r(16)$ and $s(14)$ emission lines (Fig. 2). When the excitation energy is close to the $r(16)$ line, the resonant enhancement of $v_1(2)$ is clearly observed. A decrease of this resonance as the excitation is brought to the low-energy side of $r(16)$ is seen, followed by another resonance on $v_2(1)$ when the excitation energy is close to the $s(14)$ line. Out of resonance, i.e., for excitation energy set above $r(16)$ or between $s(14)$ and $s_4(10)$, only $v(3)$ or v_3 are weakly excited. Light absorption on $r(16)$ and $s(14)$ is then followed by selective excitation transfer down to $v_1(2)$ and $v_2(1)$, the nearest lines (v_3 and v) not being involved. The selective excitation transfer thus arises from thermalization between excited and ground electronic states of the same bound-exciton complex (BEC). Two defect centers related to, respectively, $v_2(1)$-$s(14)$ and $v_1(2)$-$r(16)$ are then evidenced. The observation of the other low-lying emission lines indicates that several distinct defect centers are expected to be involved in the 1.504–511-eV emission band. The PL excitation of the low-energy group of lines associated with the low-lying states of distinct defect centers will be a straightforward way to detect the sets of the relevant upper energy states.

A. Selective transfer to v_3

The excitation spectrum recorded for the v_3 line in Fig. 3 demonstrates the strong resonance on the t^* line (not defined on the SR-type PL spectrum): the t^* excitation peak intensity decreases when the luminescence energy is taken just below or above the v_3 line. The $u(8)$ and $s_4(10)$ lines are not observed as excitation peaks and there are no other lines in the g-v region which show resonance, even if some of them are weakly detected. Reciprocally, the v_3 resonance is confirmed by SPL spectroscopy when the excitation light is set in spectral region around the t line. The resonance on the t^* line is sharp, its width being comparable with that corresponding emission line (Fig. 3), whereas v_3 is much broader and overlaps the close $v_2(1)$ emission band. The off-resonance SPL spectra of Fig. 3 recorded for excitation energies set

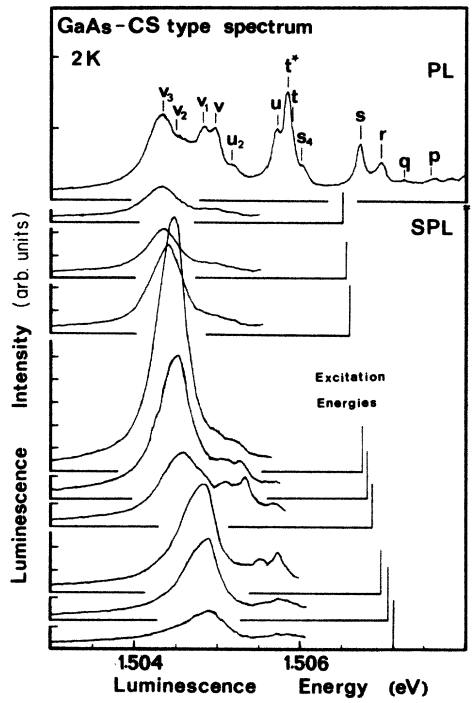

FIG. 2. Photoluminescence (PL) and selectively excited photoluminescence (SPL) of CS-type sample. A resonant excitation on the $s(14)$ and $r(16)$ emission lines leads to selective excitation transfers down to the $v_2(1)$ and $v_1(2)$ low-lying states, respectively. The $u(8)$, t^*, $t(9)$, and $s_4(10)$ intermediate states are very weakly populated.

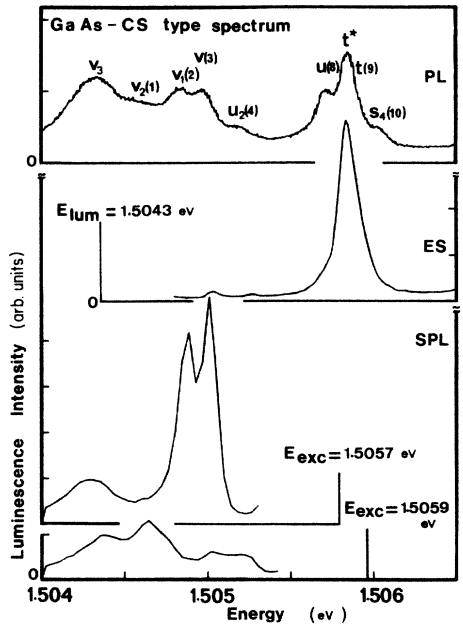

FIG. 3. Excitation-transfer processes between $u(8)$, t^*, $t(9)$, and the low-energy lines of the growth-induced emission band observed in CS-type samples. The excitation spectrum (ES) of the v_3 line demonstrates a strong resonance on the t^* line. The SPL spectrum excited at 1.5057 eV, between t^* and $u(8)$, shows transfers down to v_3 from t^* and to $v_1(2)$ and $v(3)$ from $u(8)$. The $v_2(1)$ line is enhanced by selective excitation near $t(9)$ at 1.5059 eV. The spectra are recorded with circularly polarized excitation light.

on both sides of t^* show a slight shift of the maximum of the broadened v_3 emission band, which indicates that several electronic states could be involved. Different processes may account for the excitation transfer from t^* to v_3 depending on how it occurs, either between distinct sites by exciton hopping or between ground and upper excited states of a single defect (i.e., intracenter recombination). However, exciton-transfer processes between distinct defects from site to site seem inconsistent with the correlated appearance of v_3 and t^* in the g-v emission band, especially as no transfer from any other lines toward v_3 was detected. On the other hand, in an intracenter recombination scheme, where t^* would be identified as an excited state located at 1.49 meV above the v_3 ground exciton level, special conditions have to be assumed on the thermalization processes down to v_3 in order to take into account the relative strength of the t^* line in respect to the v_3 intensity, at low temperature. However, since similar behaviors are observed for the other low-energy lines, the intracenter model more than adequately describes the g-v emission-band properties.

B. Selective transfer to v_2

The v_2 system is proving much more complicated than the v_3 one, which consists of only two levels. The excitation spectrum of $v_2(1)$ recorded with circularly polarized excitation light [Fig. 4(a)] shows the resonances on $t(9)$, $s(14)$, $p(19)$, and $k^*(26a)$. The $n(22)$ line intensity reaches its maximum for a luminescence energy set at 1.5047 eV between the $v_2(1)$ and $v_1(2)$ lines, and therefore is attributed to another system whose ground state is labeled v_2^*. The $r(16)$ and $i(30)$ lines are rising and will be resonant on the $v_1(2)$ line.

As shown in Fig. 5, ES of the v_2 line recorded with linearly polarized excitation light shows the enhancement of the resonance of the $s(14)$ and $p(19)$ lines, when the laser polarization is parallel to the $[\bar{1}10]$ direction, whereas $k^*(26a)$ is maximum in the [110] one. The fact that the strongly polarized absorption lines are those which have been unambiguously demonstrated also to be polarized in emission as well in the CS-type spectrum as in the SR-type one is striking. The $t(9)$ line is found to be unpolarized in absorption as well as in emission. The $n(22)$ line was reported as being $[\bar{1}10]$-polarized in the SR-type layers.[15]

The transfer features down to $v_2(1)$ which are drawn from ES experiments, are checked on by PL spectra selectively excited close to $s(14)$, to $t(9)$, to $k^*(26a)$, and to $p(19)$, respectively, in Figs. 2, 3, 4, and 6. Excitation near $k^*(26a)$ simultaneously gives rise to resonances on $v(3)$ and $v_2(1)$. The laser-beam linewidth (0.08 meV) is frequently more broader than two close, narrow excited states, $k^*(26a)$ and $k(27)$, which belong, respectively, to the v_2 and v systems, and which are separated by only 0.04 meV.

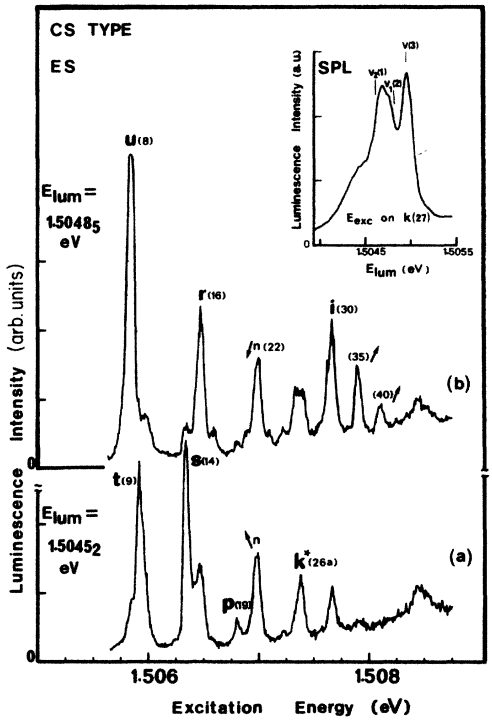

FIG. 4. Excitation spectra of (a) $v_2(1)$ and (b) $v_1(2)$ recorded for circularly polarized excitation light. The bold type denotes the resonant excitation peaks, whereas the off-resonance ones are distinguished by oblique arrows. The $t(9)$, $s(14)$, $p(19)$, and $k^*(26a)$ are resonant with the $v_2(1)$ luminescence line, and $u(8)$, $r(16)$, and $i(30)$ are resonant with $v_1(2)$. All the other lines are off resonance. For instance, the maximum intensity of $n(22)$ is obtained when the detection energy is set on v_2^*, an extra line between $v_2(1)$ and $v_1(2)$. Reciprocally, excitation on $k(27)$, at 0.04 meV near $k^*(26a)$, shows the resonances on $v(3)$ and $v_2(1)$.

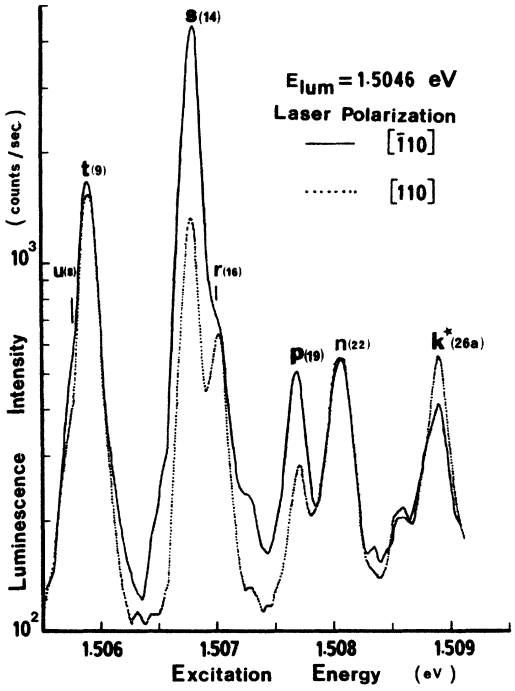

FIG. 5. Excitation spectra of $v_2(1)$ obtained for linearly polarized excitation parallel to [1̄10] (solid line) and to [110] (dotted line). $s(14)$ and $p(19)$ are [1̄10]-polarized perpendicularly to the $k^*(26a)$ polarization. The resonance on $p(19)$ is much more marked than in the circularly polarized ES of Fig. 4. The absorption on $t(9)$ is insensitive to the polarization of the light.

C. Selective transfer to v_1

The excitation spectrum of $v_1(2)$ shows [Fig. 4(b)] that recombinations at $v_1(2)$ are supplied by absorption transitions at $u(8)$, $r(16)$, and $i(30)$. The other lines are either decreasing as $n(22)$ and $k^*(26a)$ or increasing as $k(27)$, (35), and (40) accordingly as their maxima are reached for luminescence energy selected in the lower or upper side of $v_1(2)$. In the v_1 system, $u(8)$ is the only [1̄10]-polarized emission line, although in the SR-type spectrum $r(16)$ has been found to be slightly [1̄10]-polarized.[15] The weakness of the $i(30)$ emission line obfuscates any conclusion about its polarization behavior. In addition, the $u(8)$ excitation peak exhibits the same feature (Fig. 7) as in emission.

Resonant transfer from $u(8)$ and $r(16)$ toward $v_1(2)$ are confirmed from SPL spectra, respectively, on Figs. 2 and 3. The PL spectra selectively excited on the $i(30)$ line (inset of Fig. 7) show the resonance on $v_1(2)$. The excitation of $v(3)$ is due to the closeness of an extra line from $i(30)$, labeled $i^*(29)$, which belongs to the $v(3)$ system.

D. Selective transfer to v

The greater number of associated lines, especially with several nearby unlike levels, entails additional complications in the v system. We have already seen that the resonant excitations of $i(30)$ in Fig. 7 and $q(17)$, in Fig. 6(b), populate the $v(3)$ state. Then, the excitation spectra of

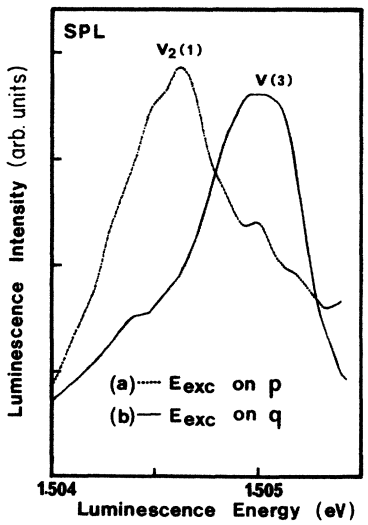

FIG. 6. SPL spectra selectively excited (a) on $p(19)$ (dotted line) and (b) on $q(17)$ (solid line).

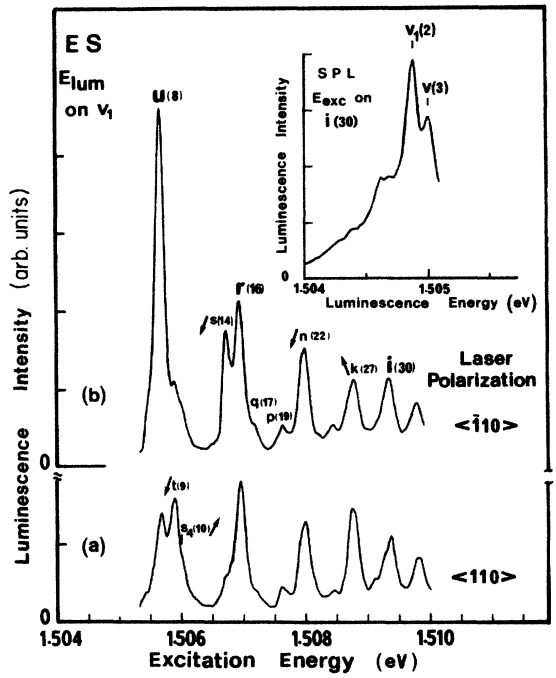

FIG. 7. Excitation spectra recorded for $v_1(2)$ with excitation light linearly polarized (a) in the [110] direction and (b) in the [$\bar{1}$10] one. The resonant $u(8)$ excitation peak is strongly polarized in the [$\bar{1}$10] direction, whereas the intensity of the remaining $r(16)$ and $i(30)$ lines of the v_1 system is not dependent on the polarization of the excitation. The SPL spectrum in the inset with the excitation tuned on the $i(30)$ line shows the resonance on $v_1(2)$. Note also the weak excitation of the $v(3)$ line caused by the closeness of $i^*(29)$ with the selectively excited $i(30)$ line.

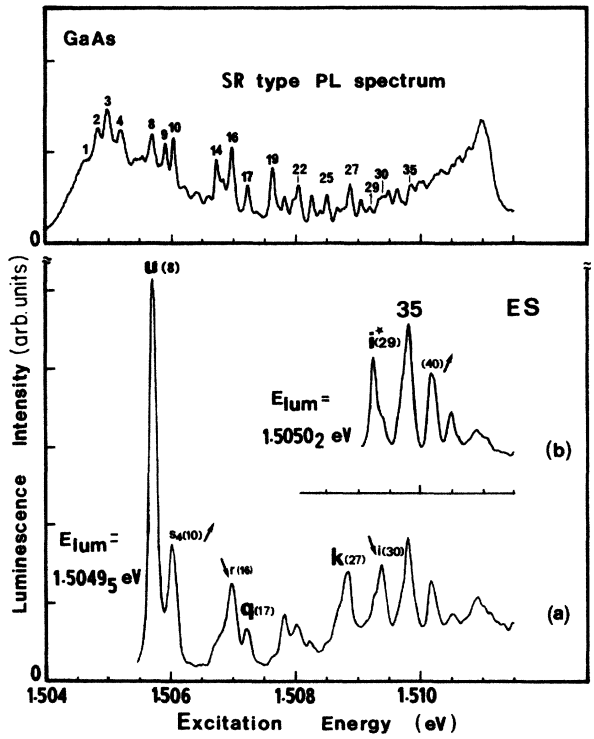

FIG. 8. Excitation spectra of the $v(3)$ line for circularly polarized excitation light with the detection, respectively, set (a) close to $v(3)$ and (b) on the high-energy side of $v(3)$. The SR-type PL spectrum allows an accurate determination of the excitation-peak location. The resonances are $u(8)$, $q(17)$, $k(27)$, $i^*(29)$, and line (35).

$v(3)$ shown in Fig. 8 allow one to distinguish now all of its participating states, which are $u(8)$, $q(17)$, $k(27)$, $i^*(29)$, and line (35). A detailed and appropriate comparison of these resonant excitation peaks is suitably made, with the corresponding emission band in the SR-type spectrum on which the upper lines are most intense otherwise well defined. The $u(8)$ line is again resonant with exact coincidence. Line (35) and $q(17)$ are both enhanced here to their maximum intensity. The resonance on $k(27)$ begins [Fig. 4(b)] when the luminescence energy is set on $v_1(2)$, the intensity ratio between $k^*(26a)$ and $k(27)$ starting to be inverted after going beyond the resonance of $v_2(1)$ with $k^*(26a)$. In the same way, $i^*(29)$ is rising [Fig. 7(a)], and reaches its maximum with the luminescence energy taken on the high-energy side of the $v(3)$ line [Fig. 8(b)] before quickly decreasing when the detection is set on $u_2(4)$.

E. Some concluding remarks on experimental grounds

A common feature of the v_2, v_1, and v systems is that several excited states do not correspond to any emission line in the CS-type spectrum. Consequently, the related upper lines have been designated by the starred labels of the closest line and the corresponding numerical symbol used on the SR-type spectrum. It should be noted that few lines in the whole 1.504–1.511-eV emission band are involved in the four systems related to the v_3, $v_2(1)$, $v_1(2)$, and $v(3)$ low-energy lines. A set of other upper states has been found to be connected to the low-lying $u_2(4)$ line, but at the present time the complexity of the results has made any definite description of the u_2 system unclear. The same holds true for the lines (5), (6), and (7), likely related to different ground electronic states. These latter lines, as well as some of the intermediate upper ones, underlie a broad emission band labeled Δ which has been previously reported[16] as a replica of the $g(47)$ line. Consequently, the number of distinct BE complex systems could be raised at least to nine.

The clearly discriminated groups include several intense lines already studied through Zeeman spectroscopy by Skolnick.[18] All the most intense lines were split into a doublet for magnetic field H set successively parallel to the [$\bar{1}$10], [110], and [001] directions, the polarization being observed for E parallel to the [$\bar{1}$10] one. From the difference in the anisotropical behavior of several lines, they had been classified into two groups: the so-called α set, which has a doublet-splitting feature for all H rotated in the ($\bar{1}$10) plane from the [001] to the [110] directions, and the β one, which exhibits a four-component splitting

for H between [001] and [110]. In agreement with Skolnick, a splitting of the $s(14)$ into a doublet has been observed for E and H parallel to $[\bar{1}10]$ and the deduced diamagnetic shift rate is 6×10^{-4} meV/kG^2, leading to an effective-mass value $m_{\text{eff}}=0.068m_0$ very close to that of the free electron in GaAs (Ref. 41) ($m_{\text{BC}}=0.067m_0$). Therefore, the bound-exciton complex is donorlike, the electron being weakly bound. Finally, the lines of the same group distinguished by ES and SPL experiments are found either in the α group or the β one, upon comparison with the symmetry-related classification.[18] For example, the $s(14)$ and $p(19)$ lines belonging to the same BE complex (v_2 system) are both of α type (rhombic I symmetry). In the same way, $q(17)$ and $k(27)$ related to the v system are α type.

IV. QUANTITATIVE INVESTIGATIONS OF THE SPLITTING PATTERN

Five systems of bound-exciton complexes (BEC's) are identified through the above resonant excitation experiments. The so-discriminated BEC's are therefore related to distinct radiative centers. Several transitions are found to be polarized, thereby reflecting the anisotropic behavior of the involved complex defects. A $J=0$ angular momentum for the final state of the BE recombination is a common feature of the optical transition.[18] Such a property is required for several kinds of traps, such as a double acceptor,[42] distant donor-acceptor pairs,[43] isoelectronic impurities,[44] and even more complicated associates.[2,45] The present section focuses on the electronic sublevel splitting of the four growth-induced BEC's, and an isoelectronic-like character will be assumed for the related traps. It will be shown that it leads to a good approach for a quantitative treatment of the BEC electronic structure. The model of isoelectronic center in a lower symmetry is the simplest one and it will be observed that it accounts for all the experimental results. A detailed investigation of the fine structure of each series of excitonic sublevels will be made in order to propose a geometrical configuration for each defect center.

The isoelectronic exciton consists of one hole related to the topmost of the valence band and of one electron related to the conduction band. The binding mechanism of the exciton obeys the Hopfield-Thomas-Lynch (HTL) model.[46] Explicitly, the isoelectronic defect presents a short-range attractive potential and this traps the hole (electron); then the electron (hole) is bound via the long-range Coulomb interaction, created by the extra density of charge associated with the localized trapped hole (electron). The prototypes of isoelectronic impurities are nitrogen in GaP (the short-range isoelectronic potential is attractive for the electron) (Ref. 47) and bismuth in GaP (the short-range isoelectronic potential is attractive for the hole).[48] The weak binding energy of the electron in the excitonic complex, established from the observed large diamagnetic shift, is a clear indication that the trap corresponding to the $s(14)$ recombination line displays a short-range potential attractive for the hole and thereby presents a bismuth-like character. To this corresponds a small effective hole Bohr radius; furthermore, the electron effective Bohr radius is larger because the electron is more weakly bound and has a smaller effective mass than the hole; as a consequence, the diamagnetic shift is close to that of the host crystal.

Let us now investigate the splitting patterns in the case of the four series of optical transitions. The standard isoelectronic exciton in a spherical semiconductor will be a starting model. The symmetry of the exciton states can be obtained by coupling the $J_h=\frac{3}{2}$ angular momentum of the bound hole (related to the topmost of the p-type valence band) and the $j_e=\frac{1}{2}$ angular momentum of the bound electron (associated to the s-like conduction band). Two levels of total angular momentum $J=1$ (dipole-allowed state) and $J=2$ (dipole-forbidden state) are obtained. The energy separation between the two levels is the spherical J-J coupling. In the more realistic case of a cubic semiconductor with a Γ_6 conduction band and a fourfold Γ_8 valence band, the exciton states are represented by $\Gamma_3+\Gamma_4+\Gamma_5$.[49] Here, Γ_5 represents the dipole-allowed state, whereas Γ_3 and Γ_4 represent the dipole-forbidden spin-triplet states.

The energy separation between these three levels can be obtained after the resolution of the exchange interaction, which can be described by the following Hamiltonian:[50]

$$H_{\text{exch}}=\tilde{\Delta}_1(J_hJ_e-\tfrac{3}{4})+\tilde{\Delta}_2(J_{hx}^3J_{ex}+J_{hy}^3J_{ey}+J_{hz}^3J_{ez})\ .$$

$\tilde{\Delta}_1$ and $\tilde{\Delta}_2$ represent the isotropic and anisotropic spin-exchange splitting. $\tilde{\Delta}_2$ is a cubic correction which is vanishingly small in the case of free excitons[50] or nitrogen bound excitons.[51] In the case of an isoelectronic potential attractive for the hole, $\tilde{\Delta}_2$ is no longer negligible.[48] The basis functions of interest which transform like Γ_3, Γ_4, and Γ_5 are linear combinations of the spherical harmonics:

$$\Gamma_5:\quad |x\rangle=(|1,1\rangle-|1,\bar{1}\rangle)/\sqrt{2}\ ,$$
$$|y\rangle=(|1,1\rangle+|1,\bar{1}\rangle)/i\sqrt{2}\ ,$$
$$|z\rangle=-|1,0\rangle\ ;$$

$$\Gamma_3:\quad |2+\rangle=(|2,2\rangle+|2,\bar{2}\rangle)/\sqrt{2}\ ,$$
$$|2,0\rangle\ ;$$

$$\Gamma_4:\quad |1+\rangle=-(|2,1\rangle+|2,\bar{1}\rangle)/\sqrt{2}\ ,$$
$$|1-\rangle=i(|2,\bar{1}\rangle-|2,1\rangle)/\sqrt{2}\ ,$$
$$|2-\rangle=(|2,2\rangle-|2,\bar{2}\rangle)/\sqrt{2}\ .$$

It is then a straightforward exercise to obtain the eigenenergies of interest:

$$E(\Gamma_5)=\tfrac{5}{8}\tilde{\Delta}_1+\tfrac{41}{16}\tilde{\Delta}_2\ ,$$
$$E(\Gamma_3)=-\tfrac{3}{8}\tilde{\Delta}_1-\tfrac{39}{16}\tilde{\Delta}_2\ ,$$
$$E(\Gamma_4)=-\tfrac{3}{8}\tilde{\Delta}_1-\tfrac{15}{16}\tilde{\Delta}_2\ .$$

The exciton states can be described by a diagonal 8×8 matrix. Any lowering of cubic symmetry will split at

least Γ_4 and Γ_5 because the threefold degeneracy can only be obtained in the cubic symmetry. The corresponding matrix can be obtained from the unified treatment of Cho,[52] appropriately modified to the problem under consideration.

In the appendix we give a detailed algebraic description of the symmetry properties of the exciton states in both cases of isoelectronic excitons and double-acceptor bound excitons. The number of expected sublevels is shown either in the cubic symmetry or in the lowered C_{3v} one. The experimental observation of two up to six excitonic levels in the various BEC's supports the isoelectronic model that will be used further.

A. The v_3-t^* system

This is a simple system which consists of a sharp unpolarized t^* line at higher energy than the v_3 low-energy transition. The width of the v_3 line (0.38 meV) is larger than that (0.16 meV) of the t^* line; as a consequence, the t^* line may be associated with Γ_5 and the v_3 band with Γ_3-Γ_4. This is a situation close to bismuth bound excitons. The Γ_3-Γ_4 quintet can only be observed because of thermalization effects and it is expected to have a long radiative lifetime. The values of the corresponding splitting parameters are $\tilde{\Delta}_1 = 1.45$ meV and $\tilde{\Delta}_2 = 0.04$ meV. The value of $\tilde{\Delta}_2$ has been estimated from the width of the v_3 line. No anisotropic character can be evidenced for the trap responsible of the v_3 and t^* recombination lines.

B. The v_1-u-r-i system

The system consists of four recombination lines. Thus, its description is consistent with a trigonal C_{3v} lowering of symmetry. The valence-band states are split by this local field and the magnitude of such a splitting can be quantitatively described with a phenomenological parameter E_1 reflecting the anisotropy of the local field in the [111] direction. The splitting of the p-like states can be written in both the local group axis and in the crystallographic axes,[53]

$$\begin{matrix} P_{[1\bar{1}0]} & P_{[11\bar{2}]} & P_{[111]} \end{matrix} \qquad \begin{matrix} P_x & P_y & P_z \end{matrix}$$

$$\begin{bmatrix} -E_1 & 0 & 0 \\ 0 & -E_1 & 0 \\ 0 & 0 & 2E_1 \end{bmatrix}, \qquad \begin{bmatrix} 0 & E_1 & E_1 \\ E_1 & 0 & E_1 \\ E_1 & E_1 & 0 \end{bmatrix}.$$

Using the theoretical treatment of Cho,[52] the excitonic matrix in the cubic basis can be written in the following form:

$$\begin{array}{cccccccc} \Gamma_3 & \Gamma_3 & \Gamma_4 & \Gamma_4 & \Gamma_4 & \Gamma_5 & \Gamma_5 & \Gamma_5 \\ |2+\rangle & |2,0\rangle & |1+\rangle & |1-\rangle & |2-\rangle & |x\rangle & |y\rangle & |z\rangle \end{array}$$

$$\begin{bmatrix} -\frac{3}{2}\tilde{\Delta}_1 - \frac{39}{16}\tilde{\Delta}_2 & 0 & -i\sqrt{3}E_1 & i\sqrt{3}E_1 & 0 & -iE_1 & -iE_1 & 2iE_1 \\ & -\frac{3}{8}\tilde{\Delta}_1 - \frac{39}{16}\tilde{\Delta}_2 & iE_1 & iE_1 & -2iE_1 & -i\sqrt{3}E_1 & -i\sqrt{3}E_1 & 0 \\ & & -\frac{3}{8}\tilde{\Delta}_1 - \frac{15}{16}\tilde{\Delta}_2 & \sqrt{3}E_1 & \sqrt{3}E_1 & 0 & E_1 & -E_1 \\ & & & -\frac{3}{8}\tilde{\Delta}_1 - \frac{15}{16}\tilde{\Delta}_2 & \sqrt{3}E_1 & -E_1 & 0 & E_1 \\ & & & & -\frac{3}{8}\tilde{\Delta}_1 - \frac{15}{16}\tilde{\Delta}_2 & E_1 & -E_1 & 0 \\ & \text{conjugate complex} & & & & \frac{5}{8}\tilde{\Delta}_1 + \frac{41}{16}\tilde{\Delta}_2 & \sqrt{3}E_1 & \sqrt{3}E_1 \\ & & & & & & \frac{5}{8}\tilde{\Delta}_1 + \frac{41}{16}\tilde{\Delta}_2 & \sqrt{3}E_1 \\ & & & & & & & \frac{5}{8}\tilde{\Delta}_1 + \frac{41}{16}\tilde{\Delta}_2 \end{bmatrix}$$

This complicated 8×8 matrix can be simplified if we make the following unitary transform:

$$\begin{bmatrix} |A\rangle \\ |B\rangle \\ |C\rangle \\ |D\rangle \\ |E\rangle \\ |F\rangle \\ |G\rangle \\ |H\rangle \end{bmatrix} \quad \begin{bmatrix} i & 0 & 0 & 0 & 0 & 0 & 0 & 0 \\ 0 & i & 0 & 0 & 0 & 0 & 0 & 0 \\ 0 & 0 & \frac{1}{\sqrt{3}} & \frac{1}{\sqrt{3}} & \frac{1}{\sqrt{3}} & 0 & 0 & 0 \\ 0 & 0 & \frac{1}{\sqrt{2}} & \frac{-1}{\sqrt{2}} & 0 & 0 & 0 & 0 \\ 0 & 0 & \frac{-1}{\sqrt{6}} & \frac{-1}{\sqrt{6}} & \frac{2}{\sqrt{6}} & 0 & 0 & 0 \\ 0 & 0 & 0 & 0 & 0 & \frac{1}{\sqrt{3}} & \frac{1}{\sqrt{3}} & \frac{1}{\sqrt{3}} \\ 0 & 0 & 0 & 0 & 0 & \frac{1}{\sqrt{2}} & \frac{-1}{\sqrt{2}} & 0 \\ 0 & 0 & 0 & 0 & 0 & \frac{-1}{\sqrt{6}} & \frac{-1}{\sqrt{6}} & \frac{2}{\sqrt{6}} \end{bmatrix} \quad \begin{bmatrix} |2+\rangle \\ |2,0\rangle \\ |1+\rangle \\ |1-\rangle \\ |2-\rangle \\ |x\rangle \\ |y\rangle \\ |z\rangle \end{bmatrix}$$

A 5×5 block-diagonal matrix can be written simply as

$$\begin{array}{ccccc} \Gamma_2(C_{3v}) & \Gamma_1(C_{3v}) & \Gamma_3(C_{3v}) & \Gamma_3(C_{3v}) & \Gamma_3(C_{3v}) \\ |C\rangle & |F\rangle & |D\rangle & |H\rangle & |A\rangle \\ & & (|E\rangle) & (-|G\rangle) & (-|B\rangle) \end{array}$$

$$\begin{bmatrix} -\frac{3}{8}\tilde{\Delta}_1-\frac{15}{16}\tilde{\Delta}_2+\sqrt{3}E_1 & 0 & 0 & 0 & 0 \\ 0 & \frac{5}{8}\tilde{\Delta}_1+\frac{41}{16}\tilde{\Delta}_2+\sqrt{3}E_1 & 0 & 0 & 0 \\ 0 & 0 & -\frac{3}{8}\tilde{\Delta}_1-\frac{15}{16}\tilde{\Delta}_2-\frac{\sqrt{3}}{2}E_1 & -\sqrt{3}E_1 & 0 \\ 0 & 0 & -\sqrt{3}E_1 & \frac{5}{8}\tilde{\Delta}_1+\frac{41}{16}\tilde{\Delta}_2-\frac{\sqrt{3}}{2}E_1 & E_1\sqrt{6} \\ 0 & 0 & 0 & E_1\sqrt{6} & -\frac{3}{8}\tilde{\Delta}_1-\frac{39}{16}\tilde{\Delta}_2 \end{bmatrix}.$$

The 8×8 matrix reduces to two tridiagonal 3×3 matrices plus two 1×1 trivial ones. Since both 3×3 matrices are identical, they have been superimposed. For completeness, the symmetry of the corresponding eigenstates has also been given. The four dipole-allowed states have Γ_1 and Γ_3 symmetry. It is clear that an analytical expression may be obtained for Γ_1 while numerical treatment will be made in the case of Γ_3 doublets.

Careful comparison between the luminescence data and the theoretical modeling suggests that we take the following values: $\tilde{\Delta}_1=3.90\pm0.15$ meV, $\tilde{\Delta}_2=-1.58\pm0.12$ meV, and $E_1=-0.32\pm0.08$ meV.

The large values of the energy differences $\tilde{\Delta}_1$ and $\tilde{\Delta}_2$ depend on both the electron-hole overlap and exchange interaction between the core functions of the atomic species which enter the formation of the trap. The large magnitudes of $\tilde{\Delta}_1$ and $\tilde{\Delta}_2$ confirm the hypothesis of a short-range binding mechanism in the case of the bound hole.

C. The v_2,t,s,p,k^* system

This is a system more complicated than those previously investigated. First, the recombination of the bound exciton gives a series of strongly polarized transitions. The $s(14)$ line, for example, is strongly polarized along the $[\bar{1}10]$ direction, the corresponding luminescence intensity decreasing noticeably if the [110]-polarized photons are selected. This behavior suggests an anisotropic local field with the main anisotropy direction lying along $[\bar{1}10]$. Second, when performing an experimental investigation of the Zeeman patterns collected at 2 K in the Voigt configuration for a $[\bar{1}10]$-oriented magnetic field, a splitting of each level into two components of identical magnitude has been observed. Such a splitting is characteristic of a lift of orientational degeneracy between [111]- and $[\bar{1}11]$-oriented defects.[54,55] These two properties suggest a C_S-type lowering of cubic symmetry and this is produced by a planar defect with a strong anisotropy in the plane of the defect. Let (Y',Z') be the plane of the defect with $Y'=[\bar{1}\,\bar{1}2]$, $Z'=[111]$, and $X'=[\bar{1}10]$ the local symmetry axe.

The local lowering of symmetry described with one main parameter E_1 can be expressed as a set of axes reflecting the geometrical configuration of our experiment, say $[\bar{1}10]$, [110], and [001].

It results in the following form for the excitonic matrix:

$$\begin{array}{cccc} |2+\rangle & |2,0\rangle & i\,|1+\rangle & i\,|X\rangle \end{array}$$

$$\begin{bmatrix} -\frac{3}{8}\tilde{\Delta}_1-\frac{39}{16}\tilde{\Delta}_2 & -2E_1 & \sqrt{6}E_1 & \sqrt{2}E_1 \\ -2E_1 & -\frac{3}{8}\tilde{\Delta}_1-\frac{39}{16}\tilde{\Delta}_2 & -\sqrt{2}E_1 & \sqrt{6}E_1 \\ \sqrt{6}E_1 & -\sqrt{2}E_1 & -\frac{3}{8}\tilde{\Delta}_1-\frac{15}{16}\tilde{\Delta}_2-\sqrt{3}E_1 & -E_1 \\ \sqrt{2}E_1 & \sqrt{6}E_1 & -E_1 & \frac{5}{8}\tilde{\Delta}_1+\frac{41}{16}\tilde{\Delta}_2+\sqrt{3}E_1 \end{bmatrix}$$

and

$$
\begin{array}{c}
\begin{matrix} |1-\rangle & |2-\rangle & |Y\rangle & |Z\rangle \end{matrix} \\
\begin{bmatrix}
-\frac{3}{8}\tilde{\Delta}_1-\frac{15}{16}\tilde{\Delta}_2+\sqrt{3}E_1 & \sqrt{6}E_1 & -E_1 & \sqrt{2}E_1 \\
\sqrt{6}E_1 & -\frac{3}{8}\tilde{\Delta}_1-\frac{15}{16}\tilde{\Delta}_2 & -\sqrt{2}E_1 & 2E_1 \\
-E_1 & -\sqrt{2}E_1 & \frac{5}{8}\tilde{\Delta}_1+\frac{41}{16}\tilde{\Delta}_2-\sqrt{3}E_1 & \sqrt{6}E_1 \\
\sqrt{2}E_1 & 2E_1 & \sqrt{6}E_1 & \frac{5}{8}\tilde{\Delta}_1+\frac{41}{16}\tilde{\Delta}_2
\end{bmatrix}
\end{array} .
$$

The two 4×4 matrices can be solved numerically. A good comparison between the experiment and this model is obtained when the following parameters are used:

$$\tilde{\Delta}_1=3.00\pm0.20 \text{ meV} ,$$

$$E_1=0.430\pm0.027 \text{ meV} ,$$

$$\tilde{\Delta}_2=0.02\pm0.02 \text{ meV} .$$

It should be noticed that a more accurate determination of these quantities can be made if the local field responsible for the v_2 system is expressed in a model using more than one phenomenological parameter E_1. According to the previous theoretical investigations of Kaplyanskii[54] and Gil *et al.*[53], a complete description of the local lowering of symmetry should need a second E_2 parameter to account for the X'-Y' anisotropy and a third one, E_3, to simulate the distortion of the angles around such defects.

Realistically, the comparison of experiment with calculation suggests a value at least 10 times smaller than E_1 for these two parameters; taking them into account cannot lead to a significantly clearer understanding of the v_2 system.

D. The *v-u-q-k-i**-(35) system

This system presents a quite equivalent sensitivity to the anisotropy of its local field in the growth plane and between the growth axis of the epitaxial layer and the growth plane; this does not lead to an easy analysis of the experimental results. From the Zeeman patterns, no correlation with a lift of orientational degeneracy can be seriously deduced. If there is one, it is certainly small and reflects a small distortion of cubic symmetry along the [111] direction. This defect exhibits a behavior which suggests a rhombic-type symmetry, probably caused by an axial defect or a planar one. In the latter case, the different partners are located further from each other than for the previous system; then the [111] character vanishes and the corresponding defect-cell correction decreases, and, consequently, so does the exciton binding energy. The exciton matrix corresponds to two 2×2 matrices plus one 4×4 diagonal matrix.

Working in the set of irreducible representations characteristic of C_{2v} symmetry given in Table I of Ref. 49, a set of analytical expressions is obtained:

$$S_{1,2}=\tfrac{1}{8}\tilde{\Delta}_1+\tfrac{13}{16}\tilde{\Delta}_2\pm[\tfrac{1}{4}(\tilde{\Delta}_1+\tfrac{7}{2}\tilde{\Delta}_2+E_1+E_2)^2+\tfrac{1}{12}(3E_1-E_2)^2]^{1/2} ,$$

$$S_{3,4}=\tfrac{1}{8}\tilde{\Delta}_1+\tfrac{13}{16}\tilde{\Delta}_2\pm[\tfrac{1}{4}(\tilde{\Delta}_1+\tfrac{7}{2}\tilde{\Delta}_2+E_1-E_2)^2+\tfrac{1}{12}(3E_1+E_2)^2]^{1/2} ,$$

$$S_5=\tfrac{5}{8}\tilde{\Delta}_1+\tfrac{41}{16}\tilde{\Delta}_2-E_1 ,$$

$$S_6=-\tfrac{3}{8}\tilde{\Delta}_1-\tfrac{15}{16}\tilde{\Delta}_2+E_1 ,$$

$$S_7=-\tfrac{3}{8}\tilde{\Delta}_1-\tfrac{39}{16}\tilde{\Delta}_2-E_1 ,$$

$$S_8=-\tfrac{3}{8}\tilde{\Delta}_1-\tfrac{39}{16}\tilde{\Delta}_2+E_1 .$$

The six $S_{1,6}$ states correspond to dipole-allowed transitions, whereas S_7 and S_8 do not. It is important to notice that the change of the sign of E_2 leads to a permutation of $S_{1,2}$ and $S_{3,4}$; as a consequence, it cannot be obtained. The set of phenomenological parameters has been found to be $\tilde{\Delta}_1=1.90+0.10$ meV, $\tilde{\Delta}_2=0.36+0.09$ meV, $E_1=0.60+0.10$ meV, and $E_2=\pm0.60+0.10$ meV.

V. DISCUSSION

The different recombination schemes with a $J=0$ final state were analyzed, attempting to account for all the experimental observations that are known at the present time on the 1.504–1.511-eV emission band. Considering an interpretation based on a donor-acceptor pair model, several arguments against it have been presented in detail.[28,34] In this section the discussion is essentially restricted to bound-exciton models. The experimental evidence of the selective behavior in the excitation-transfer processes suggests an appropriate description in terms of distinct systems resolved into ground and excited states.

First, the $g(47)$ line is not related to the low-energy lines, namely v_3, $v_2(1)$, $v_1(3)$, and $u_2(4)$. These low-energy lines have been demonstrated to be insensitive to the resonant excitation on $g(47)$, thereby proving its inefficiency to make the low-lying states populated.[16] The intermediate lines exhibit similar features, the only enhancement observed in this region, being a broad vibroniclike band labeled Δ around 1.507 eV. Moreover, a shift of $g(47)$ has been observed as a function of the dominant acceptor impurities,[56,57] whereas all the other lines are peaking at fixed energetic position. The present resonant excitation results establish a discrimination between

the four systems referred as its ground electronic v_3, v_2, v_1, and v states. The proposed model-like, i.e., isoelectronic, defect bound exciton accounts well for the fine structure of each system with regard to the number of observed lines.

For instance, the v_3-t^* system is described as being due to J-J splitting, with t^* arising from the $J=1$ triplet (Γ_5) state and v_3 from the $J=2$ quintuplet ($\Gamma_3+\Gamma_4$) state. The t^* triplet is expected to split into a σ doublet and a π singlet polarized perpendicular and parallel, respectively, to the direction of the applied magnetic field.

On the other hand, the v_1 system is described by taking into account an additional splitting caused by an axial field with C_{3v} symmetry. The resulting four dipole-allowed states are constituted by a Γ_1 singlet which corresponds to $v_1(2)$ and by three Γ_3 doublets related, respectively, to $u(8)$, $r(16)$, and $i(30)$. The observation of a two-component splitting[18] of $r(16)$ with the magnetic field H successively in the [$\bar{1}$10], [001], and [110] direction does not contradict this model. Furthermore, a splitting into four lines was observed for $r(16)$ when the magnetic field is rotated in the ($\bar{1}$10) plane, thus reflecting a lift of orientational degeneracy of such C_{3v} center. Consequently, the monoclinic symmetry observed by Skolnick for the $r(22)$ line of SR type may result from a slight anisotropy of the C_{3v} defect (CS type) in the plane perpendicular to the ⟨111⟩ axis.

Coming to the v_2 system, it is found that a defect with C_s symmetry permits a quantitative interpretation of its five lines. The $s(14)$ line was observed to split into a doublet for all directions of the magnetic field H in the ($\bar{1}$10) plane[18] and for H parallel to the [$\bar{1}$10] direction. Similar behavior was observed for the $p(19)$ line.[18] However, it is not possible to predict the expected remaining doublet splitting because of a strong mixing of the relevant states. Finally, the v system is fitted by a defect with C_{2v} symmetry. This gives singlet states, any degeneracy of different sublevels being accidental: For instance, this occurs in the permutation of $S_{1,2}$ and $S_{3,4}$ when changing the sign of E_2.

Although the CS- and the SR-type spectral features are mostly comparable, there exists, however, experimental evidence about several *different behaviors* between them. First, the v_3-t^* system is only detected in the CS-type sample. Second, selectively excited PL on all the lines of the g-v band did not exhibit, except for the phonon replica, any resonance in the 1.46–1.48-eV region. This has been attributed to a two-hole satellite in the SR-type sample.[17] Third, several upper lines that are in energetic coincidence in both CS- and SR-type spectra actually have distinct origins: For instance, the k line in the CS-type sample and the corresponding line—(27)—in the SR-type one[15] are, respectively, [110] and [$\bar{1}$10]-polarized. Moreover, line (27) has a two-hole replica,[17] whereas such features are not observed for the k line. The question arises as to whether the same upper states are involved in CS- and SR-type spectra, particularly when considering the v_3-t^* system which is predominant in the CS-type g-v emission band, whereas it is absent in the SR-type one. A partial answer may be given in comparing the symmetries found for the v_2- and v-related defects. They are, respectively, C_s and C_{2v} in the CS-type sample, whereas they are rhombic I and monoclinic in the SR-type one. This fact may indicate a different behavior with regard to the local distortion around the defects in the two samples. Anyway, the low-lying states in the CS-type spectrum correspond to distinct systems, having upper excited states with typical transfer times that are long enough to allow their detection.

The electron-hole exchange parameters have been found to exceed a milli-electron-volt in all four cases. To our knowledge, comparable values are theoretically expected[58] and measured[48] in the case of GaP. However, such large values cannot be easily obtained for GaAs in the framework of elementary Hartree calculations, due to the relative smallness of the exciton binding energy (in the 4–11-meV range).[59]

VI. CONCLUSION

Various techniques were used for a detailed understanding of properties of excitons bound to growth-induced defects. The resonant excitation experimental study demonstrates the selectivity of excitation transfers from excited to ground electronic states related to the low-lying lines in the 1.504–1.511-eV emission band. Consequently, five sets of bound-exciton recombination lines are discriminated and associated with distinct defect centers. Polarization measurements show the direct connection between several lines and oriented complex defects having a lower symmetry. The donorlike character of the excitonic complexes evidenced in this work and in Ref. 18 by magneto-optical studies reflects the short-range hole-attractive potential of the related defects. One of these systems, namely v_3-t^*, whose ground state lies lowest in the g-v band, is found to be suppressed in some type of samples (so-called SR type), depending on the MBE growth conditions. A numerical investigation of the sublevel splitting pattern for each bound-exciton complex, and assuming that the traps responsible for the luminescence exhibit a neutral charge, shows that they may be treated following an isoelectronic-like approach. Several types of defects are selected: the v_3-t^* system is found to be consistent with an isoelectronic-like defect in a cubic symmetry, whereas an axial [111]-oriented defect (C_{3v}) well accounts for the v_1-u-r-i bound-exciton complex; the v_2-t-s-p-k^* and v-u-q-k-i^*-(35) complexes are due to excitons bound to defects, probably having planar symmetry. A strong value of the electron-hole coupling is found and indicates an isoelectronic short-range potential, attractive for the hole.

ACKNOWLEDGMENTS

The authors are indebted to M. Leroux, J. Massies, and J. P. Contour for stimulating fruitful discussions. They want to express their gratitude to Le Si Dang for magneto-optical aspects of this work. Thanks are due to A. Kozacki for expert assistance in experiments and to D. Huet for providing a part of the high-quality layers.

APPENDIX

We now give a comparison between the symmetry of the excitonic states in the case of an isoelectronic exciton and in the case of a neutral double-acceptor bound exciton.

(i) The isoelectronic-center bound exciton in zinc-blende symmetry. The symmetry of the exciton states is obtained from the product of the symmetries of both the bound electron states and the bound hole states. In the case of cubic center, the exciton states split into $\Gamma_3+\Gamma_4+\Gamma_5$. A radiative recombination may occur between the Γ_5 and Γ_1 ground states. Working in the most symmetrical case of the spherical symmetry, Γ_5 corresponds to a $J=1$ total angular momentum of the exciton, $\Gamma_3+\Gamma_4$ corresponds to a $J=2$ one, split by the crystal field, and Γ_1 corresponds to the ground state of the crystal with $J=0$.

(ii) The double-acceptor bound exciton in zinc-blende symmetry. The ground state consists of a system which binds two equivalent holes. Two combinations are allowed by the exclusion principle for J-J coupling between two $J=\frac{3}{2}$ holes, namely $J=0$ and 2, which describe the electronic states of a double acceptor in a spherical III-V semiconductor. It is a straightforward exercise to obtain the symmetry of the corresponding states in a cubic semiconductor from the antisymmetric direct product $\Gamma_8\times\Gamma_8$.

From Koster's tables[49] one gets $(\Gamma_8\times\Gamma_8)=\Gamma_1+\Gamma_3+\Gamma_5$. In that case, the $J=2$ state has $\Gamma_3+\Gamma_5$ cubic symmetry and not $\Gamma_3+\Gamma_4$. The corresponding energies of these levels are *a priori* different, the energy separation depending on both the magnitude of the hole-hole coupling and the crystal-field strength.

The double-acceptor bound exciton consists of three equivalent Γ_8-like holes and one Γ_6 electron. The three holes make a $(\Gamma_8\times\Gamma_8\times\Gamma_8)$ antisymmetrical states which transform like Γ_8. Then, the double-acceptor bound exciton has $\Gamma_8\times\Gamma_6$ symmetry, like the isoelectronic bound exciton, but has, of course, different eigenstates: The recombinations then can occur between the $\Gamma_5+\Gamma_3+\Gamma_4$ states of the bound exciton and the $\Gamma_1+\Gamma_3+\Gamma_5$ levels of the double-acceptor ground state. As illustrated in Fig. 9, six transitions are expected for such a type of bound exciton in T_d symmetry.

(iii) Lowering of cubic symmetry. In the case of any lowering of cubic symmetry, both Γ_4 and Γ_5 will split because of the threefold degeneracy, which is allowed inside the cubic syngony only as a consequence; a more complicated energy pattern is expected as well as for isoelectronic bound exciton as for double-acceptor bound exciton. However, in the latter case, the ground state of the system (two equivalent holes in an antisymmetric state) will split, while there will be no splitting of the ground state in the case of an exciton trapped by an isoelectronic center. As an illustration, we have given the splitting pattern expected in the case of trigonal symmetry for these two types of excitons. Four radiative recombina-

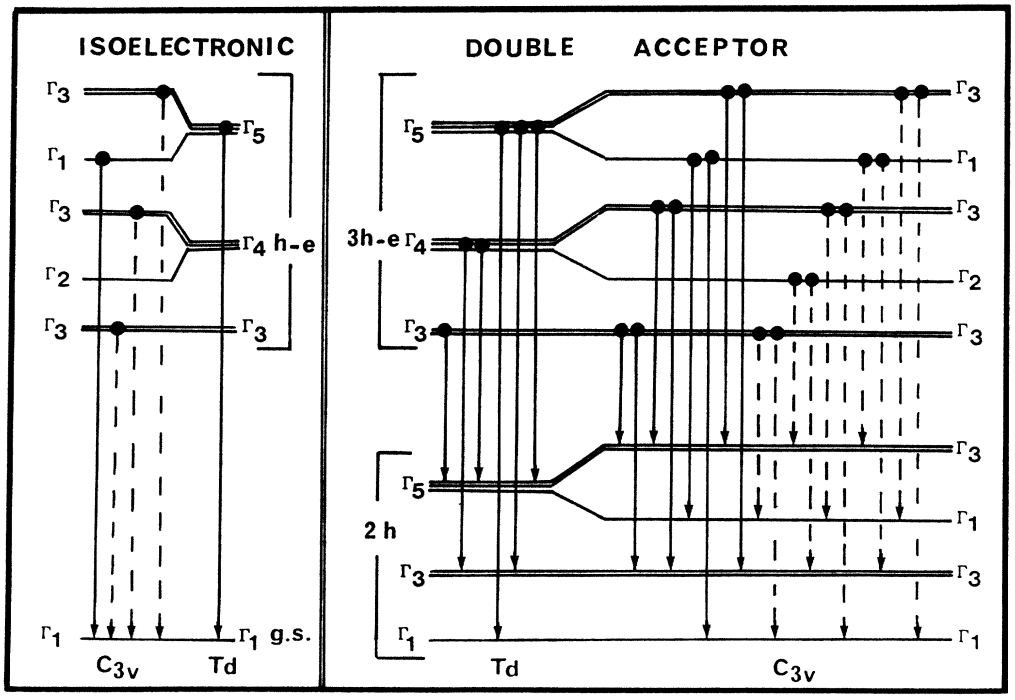

FIG. 9. Schematic picture of energy levels of excitons bound, respectively, to isoelectronic ($J=0$) and double-acceptor ($J=0$ lying lowest) centers. The $J=1$ (Γ_5) and $J=2$ ($\Gamma_3+\Gamma_4$) states of the isoelectronic bound exciton in T_d symmetry are split into three (Γ_3) doublets and two singlets (Γ_1 and Γ_2) by the C_{3v} axial field. A similar pattern is also observed for the double-acceptor bound exciton. The two hole final states in C_{3v} symmetry consist of two Γ_3 and two Γ_1 levels. The dipole-allowed recombinations are indicated by arrows for π polarization (solid lines) and σ polarization (dotted lines).

tions are expected in the case of trigonal isoelectronic center, while one may observe up to 18 in the case of double-acceptor–type axial defect with rhombic symmetry. In the case of C_{2v} axial defects, we should, respectively, predict six and 36 transitions. In the low-symmetry case of planar defects, the isoelectronic exciton would give eight levels, and, in the case of recombination of an exciton bound to a defect with two holes in its ground state, 48 transitions are predicted. In our case the number of radiative transitions has never been found to exceed six, a number reasonable with a series of isoelectronic traps.

*Permanent address: Groupe d'Etudes des Semiconducteurs, place Eugène Bataillon, 34060 Montpellier Cédex, France.

[1]H. Kunzel and K. Ploog, Appl. Phys. Lett. **37**, 416 (1980).

[2]P. J. Dean, in *Deep Centers in Semiconductors,* edited by Sokrates Pantelides (Gordon and Breach, New York, 1986), Chap. 4, pp. 185–347.

[3]P. J. Dean and D. C. Herbert, in *Excitons,* edited by K. Cho (Springer-Verlag, Berlin, 1979), Chap. 3, pp. 55–181.

[4]D. G. Thomas and J. J. Hopfield, Phys. Rev. **150**, 680 (1966).

[5]E. E. Cohen, M. D. Sturge, N. O. Lipari, M. Altarelli, and A. Baldereschi, Phys. Rev. Lett. **23**, 1591 (1975).

[6]C. H. Henry, P. J. Dean, and J. D. Cuthbert, Phys. Rev. **166**, 754 (1968).

[7]T. N. Morgan, B. Welber, and R. N. Bhargava, Phys. Rev. **166**, 751 (1968).

[8]R. A. Street and P. J. Wiesner, Phys. Rev. B **14**, 632 (1976).

[9]P. J. Dean, Phys. Rev. B **8**, 2596 (1971).

[10]P. J. Dean, D. G. Thomas, and C. J. Frosch, J. Phys. C **17**, 747 (1984).

[11]M. O. Henry, E. C. Lightowlers, N. Killoran, D. J. Dunstan, and B. C. Cavenett, J. Phys. C **14**, L255 (1981).

[12]E. C. Lightowlers, L. T. Canham, G. Davies, M. L. W. Thewalt, and S. P. Watkins, Phys. Rev. B **8**, 4517 (1984).

[13]B. Monemar, H. P. Gislason, W. M. Chen, and Z. G. Wang, Phys. Rev. B **6**, 4424 (1986).

[14]M. Leroux, G. Neu, and C. Vèrié, Solid State Commun. **5**, 289 (1986).

[15]M. S. Skolnick, T. D. Harris, C. W. Tu, T. M. Brennan, and M. D. Sturge, Appl. Phys. Lett. **46**, 427 (1985).

[16]A. C. Beye and G. Neu, J. Appl. Phys. **58**, 3555 (1985).

[17]M. S. Skolnick, C. W. Tu, and T. D. Harris, Phys. Rev. B **33**, 8468 (1986).

[18]M. S. Skolnick, in *Proceedings of the 18th International Conference on the Physics of Semiconductors, Stockholm, 1986* edited by O. Engstrom (World-Scientific, Singapore, 1987).

[19]K. Ploog, H. Kunzel, and D. M. Collins, J. Appl. Phys. **53**, 6467 (1982).

[20]H. Kunzel and K. Ploog, in *GaAs and Related Compounds, Vienna, 1980,* edited by H. W. Thim (Institute of Physics, London, 1981), p. 519.

[21]G. B. Scott, B. Duggan, P. Dawson, and G. Weigman, J. Appl. Phys. **52**, 6888 (1981).

[22]P. J. Dobson, G. B. Scott, J. H. Neave, and B. A. Joyce, Solid State Commun. **43**, 917 (1982).

[23]G. B. Scott, P. J. Dobson, G. Duggan, and P. Dawson, J. Appl. Phys. **53**, 6469 (1982).

[24]P. K. Bhattacharya, H. J. Buhlmann, and M. Ilgems, J. Appl. Phys. **53**, 6391 (1982).

[25]F. Briones and D. M. Collins, J. Electron. Mater. **11**, 847 (1982).

[26]J. P. Contour, G. Neu, M. Leroux, C. Chaix, B. Levesque, and P. Etienne, J. Vac. Sci. Technol. B **1**, 811 (1983).

[27]L. Eaves and D. P. Halliday, J. Phys. C **17**, L705 (1984).

[28]D. C. Reynolds, K. K. Bajaj, C. W. Litton, E. B. Smith, P. W. Yu, W. T. Masselink, F. Fischer, and H. Morkoç, Solid State Commun. **52**, 685 (1984).

[29]K. Akimoto, M. Dohsen, M. Arai, and N. Watanabe, Appl. Phys. Lett. **45**, 922 (1984).

[30]D. P. Halliday, L. Eaves, and P. Dawson, *Proceedings of the 13th International Conference on Defects in Semiconductors,* Transactions of the Metallurgical Society, Coronado, 1984 (AIME, New York, 1985), Vol. 149, p. 1005.

[31]E. V. K. Rao, F. Alexandre, J. M. Masson, M. Allovon, and L. Goldstein, J. Appl. Phys. **57**, 503 (1985).

[32]T. Steiner, M. L. W. Thewalt, E. S. Koteles, and J. P. Salerno, Appl. Phys. Lett. **47**, 257 (1985).

[33]B. J. Skromme, S. S. Bose, B. Lee, T. S. Low, T. R. Lepkowski, R. Y. DeJule, G. E. Stillman, and J. C. M. Hwang, J. Appl. Phys. **58**, 4685 (1985).

[34]D. C. Reynolds, K. K. Bajaj, C. W. Litton, P. W. Yu, D. Huang, J. Klem, and H. Morkoç, J. Appl. Phys. **60**, 1767 (1986).

[35]A. Y. Cho, J. Appl. Phys. **42**, 2074 (1971).

[36]B. A. Joyce, J. H. Neave, P. J. Dobson, and P. K. Larsen, Phys. Rev. B **29**, 814 (1984).

[37]P. K. Larsen, J. F. Van der Veen, A. Mazur, J. Pollman, J. H. Neave, and B. A. Joyce, Phys. Rev. B **26**, 3222 (1982).

[38]J. H. Neave, B. A. Joyce, P. J. Dobson, and N. Norton, Appl. Phys. A **31**, 1 (1983).

[39]J. Zhang, J. H. Neave, P. J. Dobson, and B. A. Joyce, Appl. Phys. A **42**, 317 (1987).

[40]The previous work of Ref. 16 had given the t symbol of Kunzel and Ploog (Ref. 1) to the emission line peaking at 1.5057_9 eV. It has been deduced from excitation experiments and an accurate comparison of the CS- and SR-type spectra that the so-called t line of Ref. 1 corresponds to a high-energy shoulder on the CS-type spectra. Consequently, the extra line at 1.5057_9 eV will be labeled t^*, while the line at 1.5058_6 eV recovers its first spelling.

[41]J. S. Blakemore, J. Appl. Phys. **53**, R123 (1982), and references therein.

[42]P. J. Dean, M. J. Kane, N. Magnea, F. de Maigret, Le Si Dang, A. Nahmani, R. Romestain, and M. S. Skolnick, J. Phys. C **18**, 6185 (1985).

[43]For a review concerning the properties of DAP, see, for instance, P. J. Dean *Inter-Impurity Recombinations in Semiconductors,* in Vol. 8 of *Progress in Solid State Chemistry,* edited by J. O. McCaldin and G. Somorjai (Pergamon, New York, 1973).

[44]D. G. Thomas, J. J. Hopfield, and C. J. Frosch, Phys. Rev. Lett. **15**, 857 (1965).

[45]The prototype of impurity which associates with other elements to make isoelectronic traps is copper. See, for instance, B. Monemar, U. Lindefelt, W. M. Chen, H. P. Gislason, and P. O. Holtz, in *Proceedings of the 18th International Conference on the Physics of Semiconductors, Stock-*

holm, 1986, Ref. 18.
[46]J. J. Hopfield, D. G. Thomas, and R. T. Lynch, Phys. Rev. Lett. **17**, 312 (1966).
[47]D. G. Thomas and M. Gershenzon, Phys. Rev. **131**, 2397 (1963).
[48]A. Onton, and T. N. Morgan, Phys. Rev. B **1**, 2592 (1970).
[49]G. F. Koster, J. O. Dimmock, R. G. Wheeler, and H. Satz, *Properties of the Thirty-Two Point Groups* (MIT, Cambridge, MA, 1963).
[50]S. Suga, K. Cho and M. Bettini, Phys. Rev. B **13**, 943 (1976).
[51]H. Mathieu, C. Bayo, J. Camassel, and P. Merle, Phys. Rev. B **22**, 4834 (1980).
[52]K. Cho, Phys. Rev. B **14**, 4463 (1976).
[53]B. Gil, J. Camassel, P. Merle, and H. Mathieu, Phys. Rev. B **25**, 3987 (1982).
[54]A. Kaplyanskii, Optispectrosk. **16**, 329 (1964).
[55]B. Gil, J. Camassel, J. P. Albert, and H. Mathieu, Phys. Rev. B **33**, 2690 (1986).
[56]Y. Makita, Y. Takeuchi, N. Ohnishi, T. Nomura, K. Kudo, H. Tanaka, H. C. Lee, M. Mori, and Y. Mitsuhashi, Appl. Phys. Lett. **49**, 1184 (1986).
[57]A. C. Beye and G. Neu (unpublished).
[58]C. Benoît à la Guillaume, Physica B + C **117&118B**, 105 (1983).
[59]C. Benoît à la Guillaume (private communication).